Zeitschrift: Schweizerische mineralogische und petrographische Mitteilungen = Bulletin suisse de minéralogie et pétrographie

Band: 83 (2003)

Heft: 1

Artikel: Infrared spectra of annite in the interlayer and lattice vibrational range

Autor: Boukili, Boubker / Holtz, François / Bény, Jean-Michel

DOI: https://doi.org/10.5169/seals-63133

Schweizerische Mineralogische und Petrographische Mitteilungen 83, 33–46, 2003

Infrared spectra of annite in the interlayer and lattice vibrational range

Boubker Boukili[1], *François Holtz*[2], *Jean-Michel Bény*[3], *Abdellah Abdelouafi*[1] and *Saida Niazi*[1]

Abstract

Fe-rich trioctahedral micas hydrothermally synthesized are characterized by infrared spectroscopy, the spectra are collected from powder suspensions. In the lattice vibrational range, the vibrations Si–O_{nb}, Si–O_b, Al–O_{nb}, Al–O–Si, Si–O–Si and δOH are all characterized by the presence of doublets in the annite KBr-absorption spectra. In agreement with observations in the vibrational range of the OH-groups, this feature is interpreted to reflect the chemical heterogeneity of the octahedral and tetrahedral layers, imposed by crystallochemical constraints. With increasing Al content of the micas along the annite-siderophyllite join, the evolution of the bands shows that Al and Si become more ordered in the tetrahedral layer. In the interlayer vibrational range, the OH-annite end-member shows clearly five of the six predicted vibrations. The bands occuring at 66 cm^{-1} and at 120–130 cm^{-1} are related to vibrations involving interlayer cation, whereas the band observed at 152 cm^{-1} is assigned to basal oxygen vibrations around the interlayer cations. The Tschermak substitution (starting from the annite end-member) increases the misfit between the octahedral and tetrahedral layers. However, variations of fO_2 do not affect significantly the band frequencies resulting from motions related to the interlayer cations, suggesting that the geometry of the interlayer site is not significantly disturbed by variation of the Fe^{3+}/Fe^{2+} ratio in annite.

Keywords: Annite, Fe-eastonite, siderophyllite, infrared absorption, lattice and interlayer infrared vibrations.

Introduction

Biotites are characterized by a large stability field and are major minerals in various geological environments. Understanding the chemical properties of these micas is important for reconstituting physical and chemical conditions prevailing during their crystallization.

Vibrational spectroscopic techniques, in particular infrared spectroscopy, are efficient tools to understand the relation between structure and chemistry of these phyllosilicates. Biotites were one of the first minerals to be investigated with infrared spectroscopy (e.g., Vedder, 1964; Wilkins, 1967; Farmer et al., 1971; Tateyama et al., 1977; Robert, 1976, 1981; Velde, 1978; Levillain and Maurel, 1980a, b; Schroeder, 1990). However, owing to the difficulties encountered in calculation of vibration frequencies, few studies have been performed on lattice and interlayer vibrations of biotites (Vedder, 1964; Ishii et al., 1967; Farmer, 1974; Tateyama et al., 1977; Velde, 1978; Robert 1976, 1981; Jenkins, 1989; Papin et al., 1997, McKeown et al., 1999) in comparison to OH stretching vibrations (Vedder, 1964; Wilkins, 1967; Russell et al., 1970; Farmer et al., 1971; Gilkes et al., 1972; Rousseaux et al., 1972; Tateyama et al., 1977; Sanz, 1976; Sanz et al., 1977, 1978; Robert, 1976, 1981; Robert et al., 1993; Levillain and Maurel, 1980a; Levillain, 1982; Velde, 1983; Boukili, 1995; Redhammer et al., 2000 etc.).

Annite as $K(Fe)_3(Si_3Al)O_{10}(OH)_2$ is the theoretical Fe-rich end-member of the trioctahedral mica and is one of the major components of natural biotites. Annite counts at least five end members (annite, oxyannite, tetraferriannite, ferrimuscovite and ferrisyderophyllite). The knowledge of the local chemistry of this phase would permit to understand the physico-chemical conditions of its crystallization. In this study, hypoaluminous iron biotites, biotites along the joins annite-siderophyllite, annite-tetraferriannite, annite-phlogopite, phlogopite-tetraferriphlogopite have been synthesized to allow a detailed characterization and assignment of infrared bands of ferrous-aluminous biotites, particularly annite, in the

[1] Faculté des sciences de Rabat, Département des sciences de la Terre, UFR geoappl, BP 1014, Rabat-Maroc. <boukili@fsr.ac.ma>
[2] Universität Hannover, Institut für Mineralogie, Welfengarten 1, D 30167 Hannover.
[3] CNRS-CRSCM, Orléans, 45071-cedex 02, France.

0036-7699/2003/83/33

lattice and interlayer vibrational range. Particular attention is also given to the influence of redox conditions to understand the effect of $^{[6]}Fe^{3+}$ and $^{[4]}Fe^{3+}$ on the infrared spectrum of annite.

Experimental methods and analytical procedures

To synthesize micas along the different end-member compositions (annite, siderophyllite, phlogopite, tetraferriphlogopite, tetraferriannite) various gels were prepared according to the method of Hamilton and Henderson (1968). These gels were used as starting material for hydrothermal synthesis of micas. Potassium was introduced as dried K_2CO_3, silicon as tetraethylorthosilicate (TEOS), aluminum and one part of iron (50%) as nitrate. Finally, metallic iron Fe° (50%) was mechanically added to the gels to obtain the appropriate bulk compositions.

The trioctahedral micas along the annite-siderophyllite join were mainly investigated in this study. Their composition can be expressed by:

$K(Fe_{3-x}\,Al_x)(Si_{3-x}Al_{1+x})O_{10}(OH)_2$

where x corresponds to the rate of the Tschermak-type substitution. In the following text, the terms annite, Fe-eastonite, Es, siderophyllite refer to following compositions:

annite:
$KFe_3(Si_3Al)O_{10}(OH)_2$; [x = 0]
Fe-eastonite:
$K(Fe_{2.5}Al_{0.5})(Si_{2.5}Al_{1.5})O_{10}(OH)_2$; [x = 0.5]
Es:
$K(Fe_{2.25}Al_{0.75})(Si_{2.25}Al_{1.75})O_{10}(OH)_2$; [x = 0.75]
Siderophyllite:
$K(Fe_2Al_1)(Si_2Al_2)O_{10}(OH)_2$; [x = 1]

Es corresponds to a composition intermediate between Fe-eastonite (x = 0.5) and siderophyllite (x = 1).

In addition to the micas of the annite-siderophyllite join, synthesis with gels along the joins annite-phlogopite, phlogopite-tetraferriphlogopite, annite-tetraferriannite and two additional hypoaluminous iron biotite compositions have also been performed.

The syntheses were done in Tuttle-type externally heated pressure vessels working vertically, with water as the pressure medium. Temperature was measured using Ni-NiCr thermocouples calibrated against the melting points of NaCl and $ZnCl_2$. Temperature uncertainty is less than ±5 °C. Pressures were measured with a Bourdon gauge, with an uncertainty of less than ±5 MPa. Experiments were performed at 600 °C, 100 MPa P_{H2O}, with a duration of 7 days. Oxygen fugacity was controlled by the double capsule methode of Eugster (1957), using the magnetite-wüstite (MW), cobalt-cobalt oxide (CCO) and nickel-nickel oxide (NNO) assemblages as solid buffers introduced with water in the external Au-capsule. In the inner capsule ($Ag_{70}Pd_{30}$), the gels were introduced with 15 wt% distilled water. Cooling was performed by removing the vessel from the furnace and a temperature of less than 100 °C was reached after less than 1 hour.

Some micas were analyzed by electronic microprobe (Cameca, SX50) to check the stoichiometry of the synthesized minerals. Analytical conditions were: acceleration voltage of 15 kV, initial beam current 30 nA, beam diameter 1 µm and counting time 10 s.

The run products were examined with a petrographic microscope and by scanning electron microscopy (SEM). X-ray diffraction was used to confirm the single phase character and to characterize the micas. Diffraction patterns were obtained between $5° \leq 2\theta \leq 65°$, the radiation used was Co-Kα (λ = 1.7902 Å). The interplanar distances d_{060} (= *b*/6) were systematically measured using Si as an internal standard.

Mid-infrared spectra (1200–350 cm^{-1}) were recorded at room temperature on a Nicolet 710 spectrometer with a Globar source, DTGS detector. The spectra were obtained from 34 scans with a resolution of 4 cm^{-1}. Far infrared spectra were recorded on a Bruker IFS 113 spectrometer using a Mylar beamsplitter of 6 and 26 µm, mercury lamp and DTGS detector. The resolution was kept to 2 cm^{-1} with time average signal collected over 200 scans. For the collection of mid-infrared spectra, samples were prepared as KBr pellets, with a mineral to KBr ratio of 5% by weight, whereas for far infrared spectra, samples were composed of 30% of the run product and 70 wt% of polyethylene. The samples are incorporated mechanically to a matrix of KBr (or polyethylene), grounded in an agate mortar and dried for 24 to 48 hours, and finally prepared as pellets. Previous tests of the preferential orientation have been performed by tilting KBr pellets, the spectra do not seem affected.

Experimental products

The products of experiments buffered by the NNO assemblage (600 °C, 100 MPa P_{H2O}) with compositions along the annite-siderophyllite join are listed in Table 1a. One synthesis of annite in presence of D_2O has also been performed at the same conditions. The products consist of composi-

tions mica with x ranging between 0.3 and 0.75. For compositions with x of 0 to 0.2, sanidine and spinel (magnetite for x = 0) have been observed in addition to mica. The proportion of mica in these run products is always above 95%. For compositions with x of 0.8 to 1, mica is found to coexist with minor amounts of spinel, corundum [identified by X-ray diffraction; characteristic peaks: (012), (104) and (113)] and kalsilite (this is the maximum number of possible phases from the phase rule).

The crystal sizes of mica are less than 2 μm and the flakes display a brown color for the compositions with x between 0 and 0.2. With increasing Al content, the mica becomes light green. The chemical analyses demonstrate that the Al-annite compositions are close to the stoichiometry of their ideal counterparts (Table 2). The offsets observed are within the expected accuracy of microprobe analysis for fine-grained particles. There is also a decrease of the lattice spacing d(060) from 1.5534 to 1.5425 Å with increasing x from 0.75 to 1. It can be noted that our results for Fe-rich compositions as well as those of Redhammer et al. (1993) performed at 3 and 5 kbar differ from previous studies (Eugster and Wones, 1962; Wones and Eugster, 1965; Nachit, 1986). In these studies, also performed at 600 °C and 100 MPa P_{H2O}, the run products were described to be mica only. This difference is probably related to the low amount of additional phases which could not be detected with the former analytical techniques. This suggests that the stability field of Fe-rich biotites determined in these previous works needs to be reconsidered, which is in agreement with other observations (Dachs, 1994; Rebbert et al., 1995; Cyang et al., 1996). For Al-rich biotites, Redhammer et al. (2000) have shown that the solubility of Al^{3+} is strongly depending on temperature and it is limited to about 0.78–0.92. Our experimental products are in agreement with the results of Rutherford (1973): the biotite solid solution is limited to Es mica with x = 0.75. For x > 0.75, the substitution:

$^{[4]}Si^{4+} + {}^{[6]}Fe^{2+} \leftrightarrow {}^{[4]}Al^{3+} + {}^{[6]}Al^{3+}$

may be not possible. Rutherford (1973) suggests that this results from the presence of Fe^{3+} in octahedral coordination. Another explanation is that there is a substitution of Fe by Al following the reaction:

$3{}^{[6]}Fe^{2+} \leftrightarrow 2{}^{[6]}Al^{3+} + {}^{[6]}\square$.

However, following Rutherford (1973) this substitution alone cannot explain the stability limits of biotite solid solution because the maximum solid solution between annite and muscovite is limited to 10% (Monier and Robert, 1986).

The products of experiments buffered by the MW assemblage (600 °C, 100 MPa P_{H2O}) obtained from gels along the annite-siderophyllite join are listed in Table 1b and are in agreement with previous studies on ferrous-aluminous biotites (Eugster and Wones, 1962; Wones, 1963b; Wones and Eugster, 1965; Rutherford, 1973; Nachit, 1986). The run products consist of mica only for compositions with $x \leq 0.75$. For $x \geq 0.8$, spinel, corundum, and kalsilite are observed as additional solid phases. The b-axis decreases with increasing x. Short b-axes are characteristic of micas containing low amounts of Fe^{3+} as has been shown by Mössbauer measurements (Levillain, 1982; Boukili et al., 1994; Boukili, 1995).

The products of the syntheses along the joins annite-phlogopite, annite-tetraferriannite, phlogopite-tetraferriphlogopite and the two additional hypoaluminous iron biotites are listed in Table 1c. In most of the products, no other phases than mica were detected from the XRD spectra (except for the annite composition and the two hypoaluminous-biotites at NNO). A detailed discussion of the crystal characteristics of these trioctahedral micas is found in Wones (1963a, b) Annersten et al. (1971) Hazen and Burnham (1973) and in Sabatier (1974), Robert and Maury (1979) for hypoaluminous iron biotite.

IR measurements in the range 200–50 cm^{-1}

The calculations of Ishii et al. (1967) on idealized structures of potassium dioctahedral and trioctahedral micas predict six infrared active vibrations in this frequency range. Two are due to the lattice vibrations, three vibrational modes are directly related to vibrations involving the interlayer cation (modes I, II, IV) and one mode involves the motion of basal oxygen vibrations around the interlayer cation (mode III). The recent calculations made by McKeown et al. (1999) on phlogopite find six frequency bands in this region, four are related to potassium vibrations. However each of the potassium vibrations is combined with those of OH-groups and octahedral cations. Ishii et al. (1967, 1969) reported far infrared absorption spectra of natural and synthetic micas and assigned the strong bands occurring in the 120–60 cm^{-1} region to K–O stretching vibrations. The same assignment was given by Tateyama et al. (1977) for bands in the range 108–71 cm^{-1} observed in potassium micas. In addition, Farmer (1974) analyzed far infrared spectra of phlogopite and muscovite and assigned the bands at 144 cm^{-1} and 150 cm^{-1} to out-of-plane K–O vibrations. The assignments adopted in the present study are based on the above cited studies and also on that

of Laperche (1991), who used dichroism absorption effects on oriented crystals and polarized IR radiation. The OH-annite end-member (x = 0) only shows clearly five of these six vibrations (Fig. 1). One band is observed at 66 cm^{-1} in annite and shifts to higher frequency as Al content of the mica increases (along the annite-siderophyllite join). The constant frequency at 90 cm^{-1} for the three most Al-rich compositions in Fig. 1 shows that these micas were saturated with respect to aluminum (the products were composed of mica and additional phases and the composition of micas did not change significantly with increasing bulk Al content of the charge). This band at 66 cm^{-1} is absent in talc and pyrophyllite but occurs at 90 and 108 cm^{-1} phlogopite and muscovite respectively (Ishii et al., 1967). Tateyama et al. (1977) and Schroeder (1990) were the first to determine a linear correlation between these frequencies and the K_{inner}–O bond lengths. On the

Table 1a Experimental products obtained at 600 °C, NNO buffer and 100 MPa P_{H2O} along the annite-siderophyllite join. Interplanar distances are measured with the accuracy of ±0.0004 Å. dt is the average cation–anion distance calculated from the relation proposed by Hazen and Burnham (1973): dt = 0.163[4][Al/(Al + Si)] + 1.608 Å. Tetragonal rotation angles (α) are calculated from the relations of Donnay et al. (1964). The lattice parameter *b* is calculated from ($b = 6 \times d_{060}$). The phases encountered are annite and aluminous biotite (Al-biotite), mica (mc), magnetite (mt), spinel (sp), corundum (cor) and kalsilite (ks). [4][Al/(Al + Si)] is the bulk atomic aluminum fraction of the starting gels.

starting compositions	Phases obtained	d_{060} (Å)	*b* (Å)	[4][Al/(Al+Si)]	dt (Å)	α (°)
annite (x = 0)						
$KFe_3(Si_3Al)O_{10}(OH)_2$	mc + san + mt	1.5534	9.3204	0.25	1.6487	2.11
$K(Fe_{2.9}Al_{0.1})(Si_{2.9}Al_{1.1})O_{10}(OH)_2$	mc + san + sp	1.5521	9.3126	0.275	1.6528	5.11
$K(Fe_{2.8}Al_{0.2})(Si_{2.8}Al_{1.2})O_{10}(OH)_2$	mc + san + sp	1.5517	9.3102	0.30	1.6569	6.62
$K(Fe_{2.7}Al_{0.3})(Si_{2.7}Al_{1.3})O_{10}(OH)_2$	Al-biotite	1.5495	9.2970	0.325	1.6609	8.32
$K(Fe_{2.6}Al_{0.4})(Si_{2.6}Al_{1.4})O_{10}(OH)_2$	Al-biotite	1.5478	9.2868	0.35	1.6650	9.60
Fe-eastonite (x = 0.5)						
$K(Fe_{2.5}Al_{0.5})(Si_{2.5}Al_{1.5})O_{10}(OH)_2$	Al-biotite	1.5465	9.2808	0.375	1.6691	10.60
$K(Fe_{2.4}Al_{0.6})(Si_{2.4}Al_{1.6})O_{10}(OH)_2$	Al-biotite	1.5449	9.2694	0.40	1.6732	11.66
$K(Fe_{2.3}Al_{0.7})(Si_{2.3}Al_{1.7})O_{10}(OH)_2$	Al-biotite	1.5448	9.2588	0.425	1.6772	12.61
Es (x = 0.75)						
$K(Fe_{2.25}Al_{0.75})(Si_{2.25}Al_{1.75})O_{10}(OH)_2$	Al-biotite	1.5425	9.2550	0.4375	1.6793	13.03
$K(Fe_{2.2}Al_{0.8})(Si_{2.2}Al_{1.8})O_{10}(OH)_2$	mc + sp + cor + ks	1.5458	9.2748	0.45	1.6813	12.79
$K(Fe_{2.1}Al_{0.9})(Si_{2.1}Al_{1.9})O_{10}(OH)_2$	mc + sp + cor + ks	1.5453	9.2718	0.475	1.6854	13.47
siderophyllite (x = 1)						
$K(Fe_2Al_1)(Si_2Al_2)O_{10}(OH)_2$	mc + sp + cor + ks	1.5448	9.2688	0.50	1.6895	14.11

Table 1b Experimental products obtained at 600 °C, MW buffer and 100 MPa P_{H2O}. Parentheses indicate trace amounts (1% or less) of the phase present. Same remarks as in Table 1a.

starting compositions	Phases obtained	d_{060} (Å)	*b* (Å)	[4][Al/(Al+Si)]	dt (Å)	α (°)
annite (x = 0)						
$KFe_3(Si_3Al)O_{10}(OH)_2$	annite + (san)	1.5553	9.3318	0.25	1.6487	0
$K(Fe_{2.9}Al_{0.1})(Si_{2.9}Al_{1.1})O_{10}(OH)_2$	Al-biotite	1.5550	9.33	0.275	1.6528	3.72
$K(Fe_{2.8}Al_{0.2})(Si_{2.8}Al_{1.2})O_{10}(OH)_2$	Al-biotite	1.5546	9.3276	0.30	1.6569	5.63
$K(Fe_{2.7}Al_{0.3})(Si_{2.7}Al_{1.3})O_{10}(OH)_2$	Al-biotite	1.5436	9.3216	0.325	1.6609	7.20
$K(Fe_{2.6}Al_{0.4})(Si_{2.6}Al_{1.4})O_{10}(OH)_2$	Al-biotite	1.5416	9.3096	0.35	1.6650	8.73
Fe-eastonite (x = 0.5						
$K(Fe_{2.5}Al_{0.5})(Si_{2.5}Al_{1.5})O_{10}(OH)_2$	Al-biotite	1.5489	9.2934	0.375	1.6691	10.17
$K(Fe_{2.4}Al_{0.6})(Si_{2.4}Al_{1.6})O_{10}(OH)_2$	Al-biotite	1.5481	9.2886	0.40	1.6732	11.08
$K(Fe_{2.3}Al_{0.7})(Si_{2.3}Al_{1.7})O_{10}(OH)_2$	Al-biotite	1.5475	9.2850	0.425	1.6772	11.77
Es (x = 0.75)						
$K(Fe_{2.25}Al_{0.75})(Si_{2.25}Al_{1.75})O_{10}(OH)_2$	Al-biotite	1.5454	9.2724	0.4375	1.6793	12.47
$K(Fe_{2.2}Al_{0.8})(Si_{2.2}Al_{1.8})O_{10}(OH)_2$	mc + sp + cor + ks	1.5459	9.2754	0.45	1.6813	12.77
$K(Fe_{2.1}Al_{0.9})(Si_{2.1}Al_{1.9})O_{10}(OH)_2$	mc + sp + cor + ks	1.5457	9.2742	0.475	1.6854	13.41
siderophyllite (x = 1)						
$K(Fe_2Al_1)(Si_2Al_2)O_{10}(OH)_2$	mc + sp + cor + ks	1.5440	9.2640	0.50	1.6895	14.23

basis of these findings and the dichroism absorption effects on oriented crystals (Laperche, 1991), we assign this band to the torsional mode of basal oxygens around the interlayer cation (mode III).

At higher wavenumbers, at least two low-resolved bands are observed in the range 120–130 cm^{-1}. They show only little variation with increasing Al content of the micas along the join annite-siderophyllite. Similar observations were made by Laperche (1991) for polarized radiation on biotites. We assign these two bands to translational vibrations of potassium in the *(a,b)*-plane (mode I et II). The calculation made by McKeown et al (1999) on phlogopite predicts also two translational vibration modes of potassium at 138 and 156 cm^{-1} combined with OH and octahedral cation vibrations. Finally, two additional low-intensity bands are observed at 152 and 183 cm^{-1}. Although

Table 1c Experimental products for additional compositions synthesized at 600 °C, 100 MPa P_{H2O} and various oxygen fugacities. Same remarks as in Table 1a and 1b.

starting compositions	Phases obtained	d_{060} (Å)	T°C/Buffer at 100 MPa P_{H2O}
annite			
$KFe_3(Si_3Al)O_{10}(OH)_2$	mc + san + mt	1.5534	600°C/NNO
$K(Fe_{2.4}Al_{0.1})(Si_3Al)O_{10}(OH)_2$	biotite	1.5475	600°C/NNO
$K(Fe_{1.8}Al_{0.2})(Si_3Al)O_{10}(OH)_2$	biotite	1.5441	600°C/NNO
$K(Fe_{1.5}Al_{0.3})(Si_3Al)O_{10}(OH)_2$	biotite	1.5433	600°C/NNO
$K(Fe_{1.2}Al_{0.4})(Si_3Al)O_{10}(OH)_2$	biotite	1.5416	600°C/NNO
$K(Fe_{0.6}Al_{0.4})(Si_3Al)O_{10}(OH)_2$	biotite	1.5407	600°C/NNO
Phlogopite			
$K(Mg_3)(Si_3Al)O_{10}(OH)_2$	phlogopite	1.5350	600°C/NNO
annite			
$K(Fe_3)(Si_3Al)O_{10}(OH)_2$	annite	1.5553	600°C/MW
$K(Fe_3)(Si_3Al_{0.8}Fe_{0.2})O_{10}(OH)_2$	biotite	–	600°C/MW
$K(Fe_3)(Si_3Al_{0.6}Fe_{0.4})O_{10}(OH)_2$	biotite	–	600°C/MW
$K(Fe_3)(Si_3Al_{0.4}Fe_{0.6})O_{10}(OH)_2$	biotite	–	600°C/MW
$K(Fe_3)(Si_3Al_{0.2}Fe_{0.8})O_{10}(OH)_2$	biotite	–	600°C/MW
tetraferriannite			
$K(Fe_3)(Si_3Fe)O_{10}(OH)_2$	ferri-annite + (mt)	1.5683	600°C/MW
Phlogopite			
$K(Mg_3)(Si_3Al)O_{10}(OH)_2$	phlogopite	1.5348	600°C/NNO
$KFe_3(Si_3Al_{0.8}Fe_{0.2})O_{10}(OH)_2$	biotite	–	600°C/NNO
$K(Mg_3)(Si_3Al_{0.6}Fe_{0.4})O_{10}(OH)_2$	biotite	–	600°C/NNO
$K(Mg_3)(Si_3Al_{0.4}Fe_{0.6})O_{10}(OH)_2$	biotite	–	600°C/NNO
$K(Mg_3)(Si_3Al_{0.2}Fe_{0.8})O_{10}(OH)_2$	biotite	–	600°C/NNO
tetraferriphlogopite			
$K(Mg_3)(Si_3Fe)O_{10}(OH)_2$	ferri-phlogopite	1.5466	600°C/NNO
annite			
$KFe_3(Si_3Al)O_{10}(OH)_2$	annite + (mt)	1.5540	600°C/CCO
hypoaluminous biotite			
$KFe_3(Si_{3.312}Al_{0.375}Fe_{0.312})O_{10}(OH)_2$	mc + qtz + p?	1.5679	600°C/NNO
$K(Fe_{2.75}\square_{0.25})(Si_{3.625}Al_{0.25}Fe_{0.125})O_{10}OH_2$	mc + qtz + san	1.5678	600°C/NNO

Table 2 Chemical composition as weight percent oxides of selected micas along the join annite-siderophyllite obtained from microprobe analysis.

Run	SiO_2	Al_2O_3	FeO	K_2O	Total
annite 600°C/NNO/100 MPa $P(H_2O)$	34.44	9.21	42.09	8.64	94.40
annite 600°C/NNO/100 MPa $P(H_2O)$	34.63	8.99	42.41	8.68	94.71
annite 600°C/MW/100 MPa $P(H_2O)$	35.20	9.43	42.20	8.63	95.46
Fe-east 600°C/NNO/100 MPa $P(H_2O)$	30.30	20.35	34.20	9.36	94.22
Fe-east 600°C/NNO/100 MPa $P(H_2O)$	30.72	20.52	35.05	9.47	95.77
Fe-east 600°C/MW/100 MPa $P(H_2O)$	30.64	19.88	36.44	9.43	96.40
Es 600°C/NNO/100 MPa $P(H_2O)$	27.23	26.20	34.05	8.59	96.07
Es 600°C/MW/100 MPa $P(H_2O)$	27.36	25.95	34.04	8.70	96.05

they are weakly resolved, these bands do not seem to be affected by compositional variations. The band at 152 cm^{-1} may be related to the mode IV, whereas the second at 183 cm^{-1} may result from lattice vibrations.

The effect of fO_2 on the bands between 150 and 50 cm^{-1} is low and no significant variations can be observed between the products obtained at the MW, CCO, NNO buffers (Fig. 2). However variations can be observed at higher frequencies with the bands assigned to lattice vibrations. With increasing fO_2, the band at 183 cm^{-1} splits into a doublet.

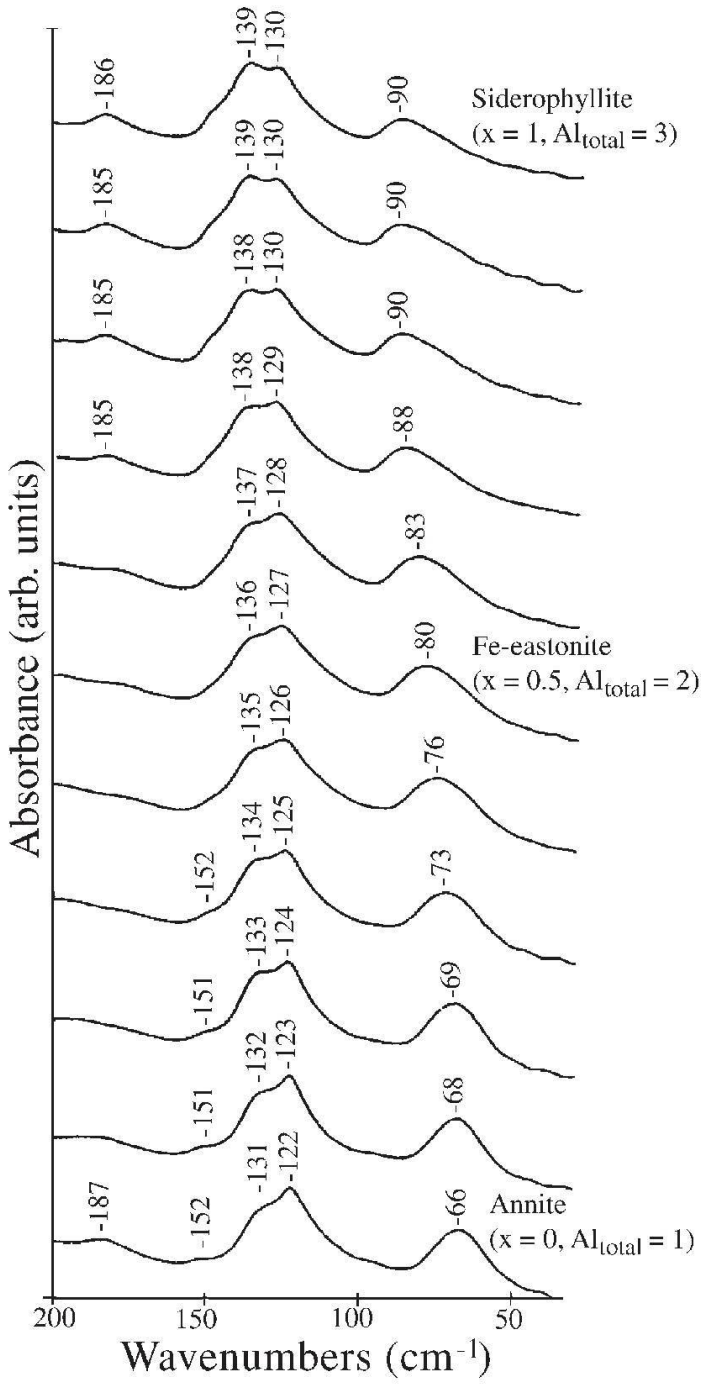

Fig. 1 Evolution of infrared spectra of annite compositions, along the annite-siderophyllite join in the frequency range of interlayer vibrations (200–50 cm^{-1}).

In summary, the evolution of far infrared K–O stretching wavenumbers (Mode III) in micas is related to the variations of geometry of the interlayer site. The interlayer cavity is approximately hexagonal in the case of annite owing to the weak dimensional misfit between the octahedral and tetrahedral layers. However, as Al is incorporated into annite, the tetrahedral rotation angle α calculated from the relations established by Tateyama et al. (1977) or by Donnay et al. (1964) increases. Thus, as for the OH $\leftrightarrow$ F substitution (Boukili et al. 1993, 2001), the Tschermak substitution (starting from the annite end member) increases the dimensional misfit between the octahedral and tetrahedral layers. However, variations of fO_2 do not significantly affect the band frequencies resulting from motions related to the interlayer cations, suggesting that the geometry of interlayer site is not significantly disturbed by a variation of the Fe^{3+}/Fe^{2+} ratio in annite.

IR measurements in the range 850–350 cm^{-1}

The absorption spectra in this frequency range are complex and result from the bending, stretching and/or combinations of Si–O and Al–O vibrations, as well as from torsional motions of OH groups (Ishii et al., 1967). Thus, it is difficult to identify exactly the vibrational modes. However, the effect of the concentration of the individual cations or of the substitutions on the bands can be understood by the analysis of the spectra along specific joins. This, in turn, allows an empirical assignment of the absorption bands.

In annite (x = 0), the peak at 763 cm^{-1} (peak labeled 1 in Fig. 3) was assigned to a tilting motion of the base of the SiO_4 tetrahedron by Redhammer et al. (2000). This peak is slightly asymmetric and results from a doublet with low intensity bands that have been assigned to an Al–O_{nb} (O_{nb} is the apical non bridging oxygen) stretching vibration by Farmer (1974). The maximum intensity of this doublets shifts toward higher frequencies (up to 825 cm^{-1}) with increasing Mg content along the annite-phlogopite join (Fig. 4). Following the assignment of Farmer (1974), a decrease of the intensity of the absorption band due to Al–O_{nb} at the expense of that due to Fe^{3+}–O_{nb} is expected along the joins annite-tetraferriannite and phlogopite-tetraferriphlogopite. By using the harmonic-approximation of IR-active vibrations, a shift factor of 1.13 is expected for the ratio of the frequencies Al^{3+}–O_{nb}/Fe^{3+}–O_{nb}. This results in a calculated frequency of 730 cm^{-1} for the Fe^{3+}–O_{nb} band in ferri-phlogopite and of 676 cm^{-1} in ferri-annite. The experimental data are in good agree-

ment with this prediction. A decrease of the band intensity at 825 cm^{-1} ($Al–O_{nb}$) at the expense of a new band at 735 cm^{-1} ($Fe^{3+}–O_{nb}$) is observed along the phlogopite-tetraferriphlogopite join (Fig. 4). Similarly, the band intensity at 763 cm^{-1} ($Al–O_{nb}$) in annite decreases at the expense of the new band at 679 cm^{-1} ($Fe^{3+}–O_{nb}$) along the annite-tetraferriannite (Fig. 4). Along the join annite-siderophyllite, the $Al–O_{nb}$ bands are progressively and clearly splitted in two contributions at 789 and 744 cm^{-1} with increasing Al content (Fig. 3, Table 3). This results from Si, Al ordering in the tetrahedral layer which is imposed by the avoidance of two adjacent $^{[4]}Al$ (Loewenstein rule), the ratio $^{[4]}[Al/(Si + Al)]$ (Bailey, 1985) and by the composition of the octahedral layers with two main octahedral environments $^{[6]}Fe^{2+}Fe^{2+}Fe^{2+}$ and $^{[6]}Fe^{2+}Fe^{2+}Al^{3+}$ toward Al-rich compositions, in agreement with the observations made in the vibrational range of OH-groups by Boukili (1995) and Redhammer et al. (2000).

The effect of fO_2 on the spectra along the annite-siderophyllite join is illustrated in Fig. 5. It can be noted that the peak at 765 cm^{-1} ($Al–O_{nb}$) in annite becomes asymmetric with increasing fO_2. This may be related mainly to the heterogeneity in the distribution of cations and vacancies in the octahedral (mainly) and tetrahedral layers ($^{[6]}Fe^{3+}$, $^{[6]}Al^{3+}$, $^{[6]}\square$, $^{[4]}Fe^{3+}$) which is imposed by crystallochemical constraints as proposed by Hazen and Burnham (1973), Dyar (1987) and Guidotti et al. (1991). In particular, annite contains more vacancies, Fe^{3+}, and intracrystalline $^{[6]}Fe^{3+}$, $^{[4]}Fe^{3+} \leftrightarrow {}^{[4]}Al^{3+}$ substitution at oxidizing conditions (Eugster and Wones 1962; Wones, 1963b; Partin, 1984; Redhammer et al., 1993; Boukili et al., 1993; Boukili, 1995; Rebbert et al., 1995).

In annite, the peak at approximatily 660 cm^{-1} results also from a doublet with a contribution at 657 and 640 cm^{-1} (band labeled 2 in Fig. 3) clearly observed in Al-poor micas. This peak has been assigned to Si–O–Mg stretching motion in phlogopite (Jenkins, 1989). Redhammer et al. (2000) have assigned these bands to Si–O–Al stretching vibrations. Along the join annite-siderophyllite, the intensity of this band clearly decreases at the expense of the Si–O–Al stretching band. Therefore, we assign this doublet to two Si–O–Si stretching vibrations probably coupled with an Si–O stretching vibration. The band occurring at 692 in phlogopite (Fig. 4) has been assigned by

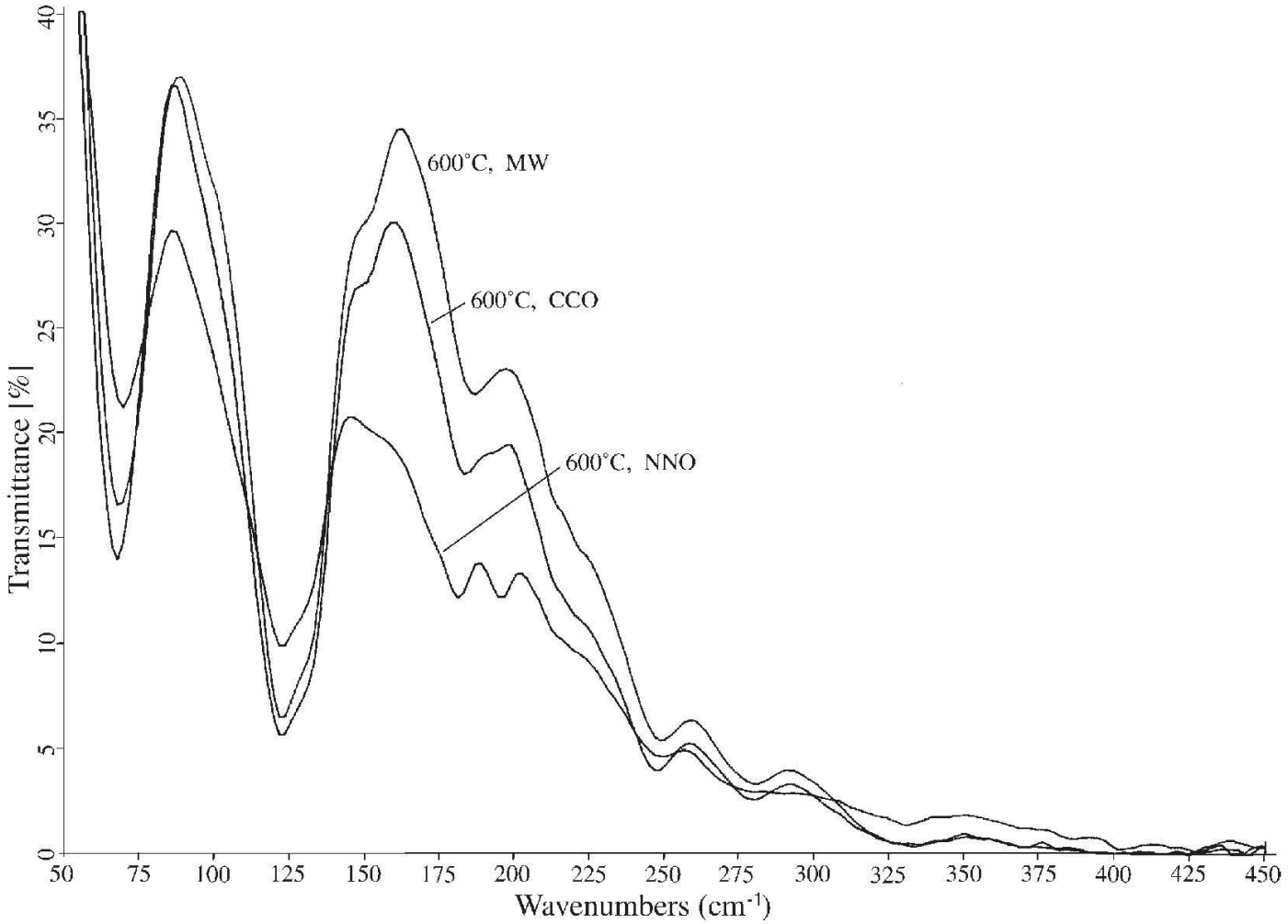

Fig. 2 Far infrared spectra of annite synthesized at 600 °C, 100 MPa P_{H2O} and the NNO; CCO; MW buffer.

McKeown et al. (1999) to T-O-T bending. Although their intensity is low, two bands at 707 and 620 cm^{-1} can be distinguished in the annite spectrum (bands labeled 3 in Fig. 3). Along the annite-siderophyllite join, the intensities of the two bands increase with increasing Al content of the mica, at the expense of the Si–O–Si bands, and the frequencies are shifted to 694 and 638 cm^{-1} for siderophyllite composition (Fig. 3, Table 4). The bands are not observed in the hypoaluminous iron micas. Along the annite-tetraferriannite and phlogopite-tetraferriphlogopite joins a shift fac-

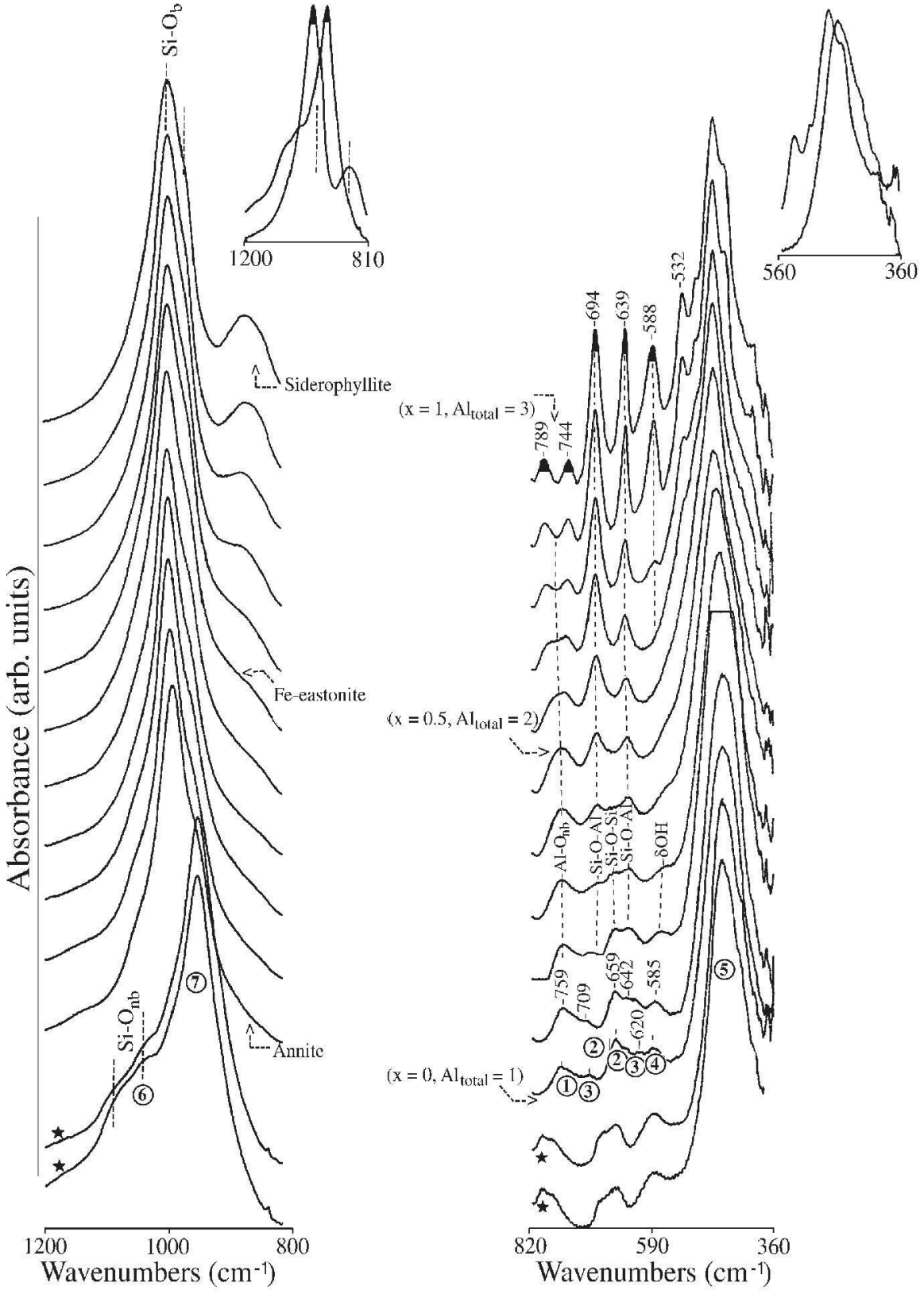

Fig. 3 Evolution of infrared spectra of annite compositions, along the annite-siderophyllite join and toward hypoaluminous iron compositions, in the frequency range of lattice vibrations (1200–800 cm^{-1} and 820–360 cm^{-1}). Hypoaluminous iron compositions are denoted with stars.

Table 3 Infrared absorptions frequencies and structural assignments suggested in this study and reported in the literature in the range 1200–350 cm^{-1}. Abbreviations: A—assignment; RI—relative intensity (vs: very strong, ms: moderately strong, s: strong, vw: very weak, w: weak); na—not assigned; (?) probable assignment. O_b are the basal bridging oxygens, O_{nb} is the apical non bridging oxygen.

Band see Fig. 3	Vedder (1964) Natural sample of biotite			Jenkins (1989) phlogopite synthetic			This study annite synthetic		
	cm^{-1}	A	RI	cm^{-1}	A	RI	cm^{-1}	A	RI
(6)	1000	Si–O	vs	–	–	–	≈1040	2×Si–O_{nb}	w
(7)	963	Si–O	vs	995	Si–O	s	≈ 997	Si–O_b	vs
(7)	905	Si–O	ms	960	Si–O	s	≈ 971	Si–O_b	vs
	–	–	–	915	Si–O	w	–	–	–
(1)	804	na	w	822	Al–O	ms	765	2×Al–O_{nb}	w
	773	na	w	760	Al–O(?)	vw	–	–	–
(3)	728	na	w	725	Al–O–Si	w	707	Al–O–Si	vw
(2)	–	–	–	–	–	–	657	Si–O–Si	w
(2)	707	na	w	690	Si–O–Mg	ms	640	Si–O–Si	w
(3)	658	na	w	655	Al–O	w	620	Al–O–Si	w
(4)	607	na	w	592	OH	ms	580	δOH	w
(4)	497	Si–O	m	520	Si–O	vs	550	δOH (?)	vw
(5)	464	Si–O	vs	495	Mg–O	vs	≈ 460	O–Si–O + M–O	–
	445	Si–O	vs	460	Si–O	vs	–	–	–
	364	na	ms	375	Si–O–Mg	ms	–	–	–

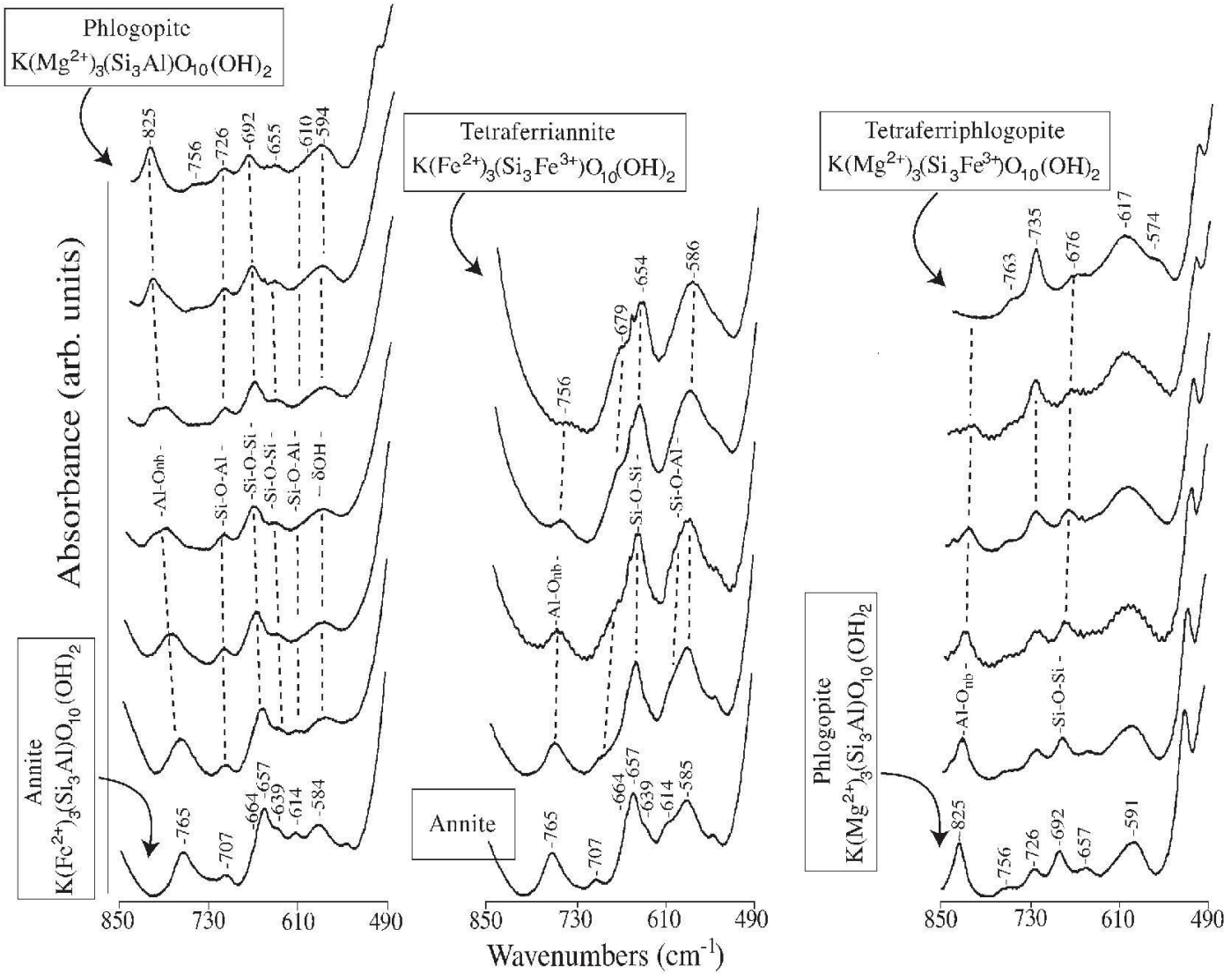

Fig. 4 Infrared spectra of annite and various chemical analogues along the annite–phlogopite, annite–tetraferriannite and phlogopite–tetraferriphlogopite joins.

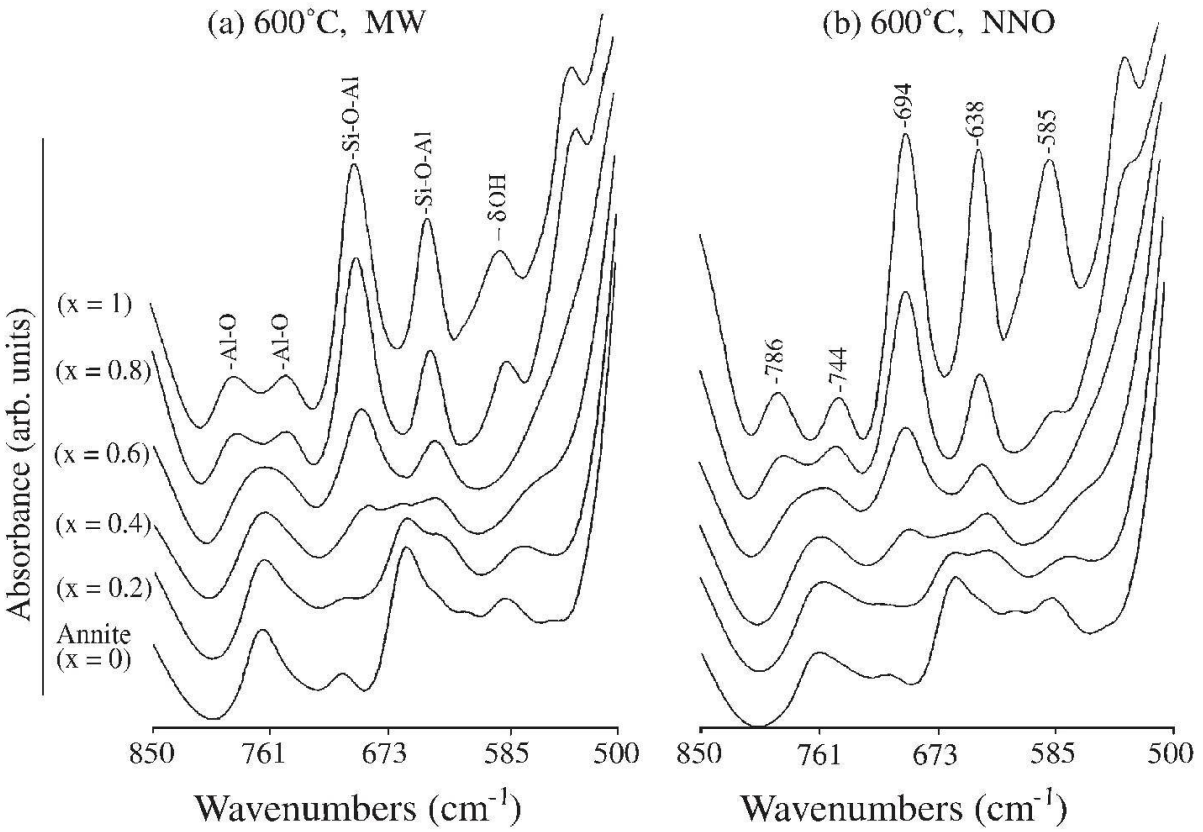

Fig. 5 Infrared spectra of micas along the annite-siderophyllite join in the range (850–500 cm^{-1}). (a) annite and Al-biotites obtained at 600 °C/MW and 100 MPa P_{H2O}. (b) annite and Al-biotites obtained at 600 °C/NNO and 100 MPa P_{H2O}.

tor of approximatively 1.13, similar to that observed from the substitution of $^{[4]}Al$ for $^{[4]}Fe^{3+}$, can be observed with increasing Al content. These observations are consistent with an assignment of these two bands to Si–O–Al stretching motions.

Thus, the intensity of bands occurring at 707 and 620 cm^{-1} (Al–O–Si) record a slight increase as the conditions become oxidizing (Fig. 6). This may relate to $^{[4]}Al \rightarrow {}^{[4]}Fe^{3+}$ substitution in agreement with Mössbauer measurements (Boukili, 1995).

The band at 580 cm^{-1} in the annite spectrum (labeled 4 in Fig. 3) corresponds to OH librational vibrations (δOH) which have been observed at 669 cm^{-1} in talc by Farmer (1974), at 600 cm^{-1} in phlogopite (Russell et al., 1970) and at 580 cm^{-1} in tetrasilicic Mg-mica (Robert et al., 1993). In the annite spectrum, a band of very low intensity at 550 cm^{-1} may also result from a second OH libration. With increasing Al content toward the siderophyllite composition, these two components corresponding to OH librations are better resolved at 588 and ≈ 532 cm^{-1}, respectively. The comparison of the spectra of OH- and OD-annite (Fig. 6) confirms the assignment of the band at 585 cm^{-1}. This band is almost absent in the spectrum of OD-annite. For comparison, the frequency range corresponding to υ_{OH} and υ_{OD} stretching vibrations is also shown in Fig. 6 and, when compared to υ_{OH}, the bands are shifted by a factor of 1.3 to 1.34 as expected. Thus, this band at 580 cm^{-1} cannot be attribued to an Al–O vibration as proposed by Redhammer et al. (2000).

It can be noted that the broad peak at approximatively 450 cm^{-1} in annite (band labeled 5 in Fig. 3) results at least from three contributions, as shown in the Al-rich compositions along the annite-siderophyllite join. The assignment of these bands can only be speculative and will not be discussed. In previous studies, they were assigned to the motions of octahedrally coordinated cations (Farmer, 1974), to Si–O vibrations coupled with an Mg–O vibrations (Jenkins, 1989), and to angular deformations of the silicate structure (O–Si–O bending vibrations) combined with stretching motions in the octahedral layer (Ishii et al., 1969).

IR measurements in the range 1200–850 cm^{-1}

The spectrum of annite exibits the features characteristic of trioctahedral micas. The spectra along the annite-siderophyllite join and of the annite end-member (x = 0, or $Al_{total} = 1$) show that the Si–O_{nb} and Si–O_b (are the basal bridging oxygens) bands are weakly resolved (bands labeled 6 and 7, Fig. 3). However, the data obtained for the two hypoaluminous iron micas show that the spectra of annite and of micas along annite-siderophyllite

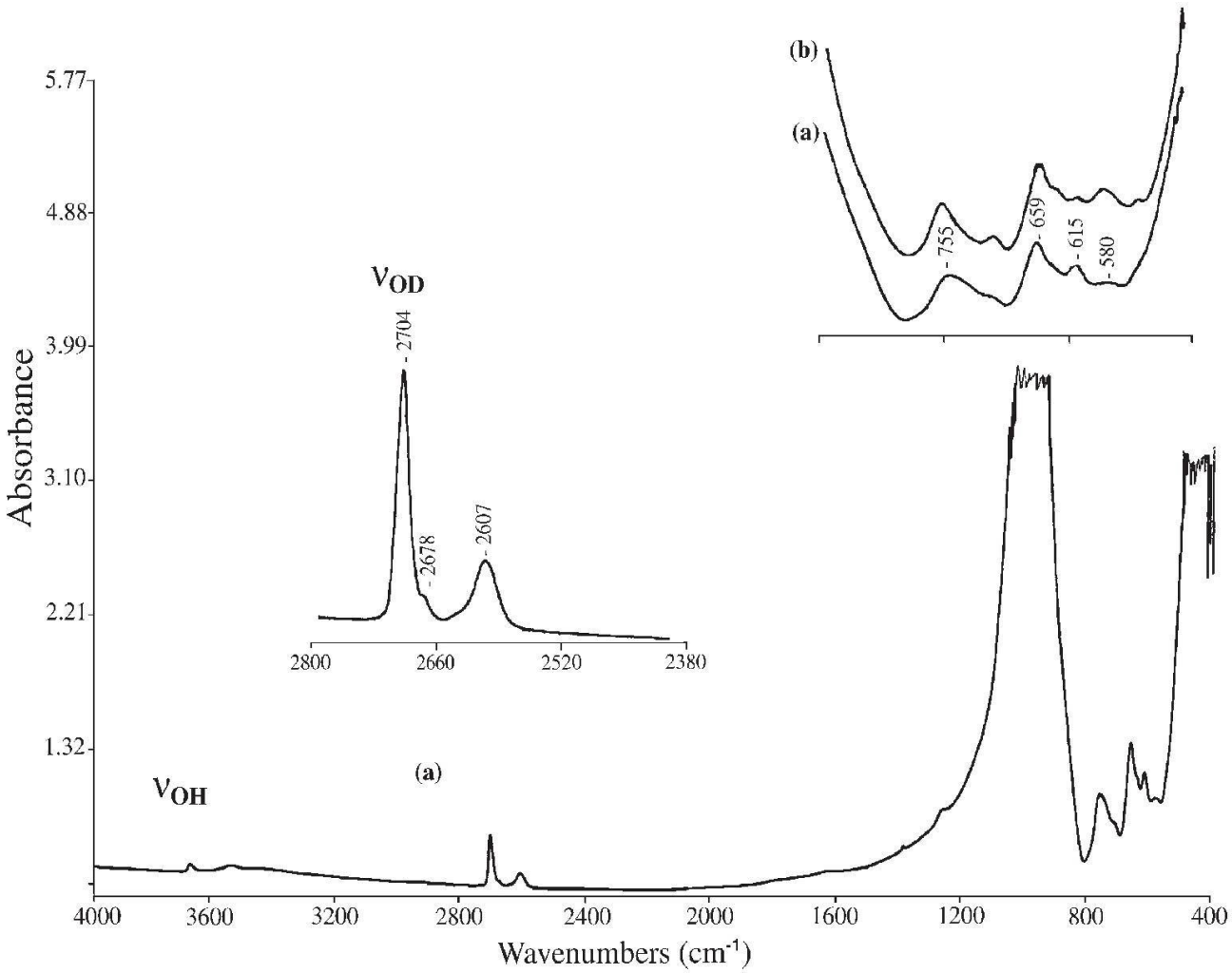

Fig. 6 Infrared spectrum of deuterated annite (a) in the range 4000–400 cm^{-1} compared to OH-annite spectrum (b).

Table 4 Infrared absorptions frequencies and structural assignments suggested in this study and reported in the literature in the lattice and interlayer vibrations range. Same abbreviations as in Table 3.

Band see Fig. 3	This study annite synthetic			This study Fe–eastonite synthetic			This study (OH)–Es synthetic		
	cm^{-1}	A	RI	cm^{-1}	A	RI	cm^{-1}	A	RI
(6)	≈ 1040	2×Si–O_{nb}	w	1035	–	w	–	–	–
(7)	997	Si–O_b	vs	995	Si–O	s	997	Si–O_b	–
(7)	971	Si–O_b	vs	965	Si–O	s	971	Si–O_b	–
(6)	–	–	w	820	Si–O_{nb}	w	873	2× Si–O_{nb}	ms
	–	–	–	–	–	–	788	Al–O	w
(1)	765	Al–O_{nb}	w	759	Al–O	w	745	Al–O	w
(3)	707	Al–O–Si	vw	694	Al–O–Si	w	694	Al–O–Si	ms
(2)	657	Si–O–Si	w	–	–	–	–	–	–
(2)	640	Si–O–Si	w	–	–	–	–	–	–
(3)	620	Al–O–Si	w	638	Al–O–Si	w	637	Al–O–Si	ms
(4)	580	δOH	w	571	δOH	vw	586	δOH	w
(4)	550	δOH (?)	vw	–	–	–	532	δOH (?)	vw
(5)	≈ 460	O–Si–O + M–O	s	≈ 460	O–Si–O + M–O	s	≈460	O–Si–O + M–O	s
	280	na	w	–	–	–	–	–	–
	240	na	w	–	–	–	–	–	–
	184	na	vw	184	na	vw	185	na	vw
	152	K–O (mode IV)	vw	150	K–O (mode IV)	ms	148	K–O (mode IV)	vw
	122–132	K–O (mode I, II)	ms	127–132	K–O (mode I, II)	ms	129–132	K–O (mode I, II)	ms
	66	K–O (mode III)	ms	80	K–O (mode III)	ms	80	K–O (mode III)	ms

need to be decomposed in four bands (Fig. 4, Table 3 and 4). Two very low-intensive (disappearing) Si–O_{nb} bands at ≈ 1040 cm^{-1} and two intense bands weakly resolved at 971 and 996 cm^{-1} (annite x = 0). The frequencies of Si–O_{nb} bands decrease with increasing Al content along the join annite-siderophyllite. This result could be attributed both to the $^{[4]}$Al–$^{[6]}$Al coupled substitution and to the increased bond valence of the M–O_3 bond in agreement with observations of Velde (1978, 1979), showing that the ratio $^{[4]}$[Al/(Si + Al)] is the main parameter controlling this frequency shift, and with further studies of Robert (1973, 1976, 1981) and Liu (1989).

In contrast to the Si–O_{nb} bands, no significant variation of the frequencies of the Si–O_b bands has been observed as a function of compositional variations along the annite-siderophyllite join.

Concluding remarks

The investigation of the evolution of infrared absorption bands along several joins involving annite as end-member allows to constrain the role of compositional variations on the frequency and the intensity of these bands. This, coupled with the effects of the fO_2 on absorption bands, is used to clarify the assignment of some characteristic absorption bands of trioctahedral micas and of annite in particular:

– The vibrations Si–O_{nb}, Si–O_b, Al–O_{nb}, Al–O–Si, Si–O–Si and δOH are found to be at 1040 and 873 cm^{-1}, at 997 and 971 cm^{-1}, at around 765 cm^{-1} (superposition of two bands), at 707 and 620 cm^{-1}, at 657 and at 640 cm^{-1}, and at 580 and 550 cm^{-1}, respectively. The presence of doublets is most probably related to the local chemical heterogeneity of the octahedral and tetrahedral sheets, which is imposed by crystallo-chemical constraints, in agreement with the observations in the vibrational range of the OH-groups. With increasing Al content of the micas along the annite-siderophyllite join, the evolution of the bands in the lattice vibration range shows that Al and Si become more ordered in the tetrahedral layer.

– In the interlayer vibrational range, the OH-annite end-member (x = 0) shows clearly five of the six predicted vibrations. One may be due to the lattice vibrations, three vibrational modes are directly related to vibrations involving the interlayer cation (modes I, II, IV) and are observed at 120–130 cm^{-1} and at 152 cm^{-1}, respectively. The band at 66 cm^{-1}, which involves the motion of basal oxygen vibrations around the interlayer cation, is assigned to the mode III.

– As for the OH ↔ F substitution, the Tschermak substitution (starting from the annite end member) increases the dimensional misfit between the octahedral and tetrahedral layers. However, variations of fO_2 do not significantly affect the band frequencies resulting from motions related to the interlayer cations, suggesting that the geometry of the interlayer site is not significantly disturbed by a variation of the Fe^{3+}/Fe^{2+} ratio in annite.

Acknowledgements

The paper has been in part financially supported by action integrée (A.I MA/01/12). I am very thankful and indebted to Dr. C. Levillain for these works on biotites. The paper benefited from the critical reviews of Prof. A. Hofmeister and an anonymous referee.

References

Annersten, H., Devanargenen, S., Haggstrom, L. and Wappling R. (1971): Mössbauer study of synthetic ferri-phlogopite $KMg_3Fe^{3+}Si_3O_{10}(OH)_2$. *Phys. Stat. Solid.* **B48**, K137–K138.

Bailey, S.W. (1985): Structural studies of clay minerals during 1981–1985. In: Schultz, L.G., Van Olfen, H. and Mumpton, A. (eds.): Proc. Intern. Clay conf., Denver, 3–8.

Boukili, B. (1995): Cristallochimie des biotites ferro-alumineuses dans le systéme: Na_2O-K_2O-FeO-Fe_2O_3-Al_2O_3-SiO_2-H_2O-HF. Analyse par spectrométries vibrationnelles et Mössbauer. Thèse, Univ. Orléans, 320 pp.

Boukili, B., Robert, J.-L. and Laperche, V. (1993): Solid solution range and crystal-chemical characterization of trioctahedral micas in the system: K_2O-FeO-Fe_2O_3-Al_2O_3-SiO_2-H_2O-HF, at 600 °C, 1 kbar. *Terra abstracts* **5**, 485.

Boukili, B., Robert, J.-L. and Beny, J.-M. (1994): Characterization of trioctahedral micas solid solutions in the system: K_2O-FeO-Fe_2O_3-Al_2O_3-SiO_2-H_2O-HF by FTIR absorption and Mössbauer spectrometries. Symp. Int. Mineral. Assoc., Pisa, Italy, OS 1–19.

Boukili, B., Robert, J.-L., Beny, J.-M. and Holtz, F. (2001): Structural effects of OH => F substitution in trioctahedral micas of the system: K_2O-FeO-Fe_2O_3-Al_2O_3-SiO_2-H_2O-HF. *Schweiz. Mineral. Petrogr. Mitt.* **81**, 55–67.

Cyang, G.L., Chou, I.M. and Sherman, D.M. (1996): Re-investigation of the annite = sanidine + magnetite + H_2 reaction using the fH_2 sensor technique. *Am. Mineral.* **81**, 475–484.

Dachs, E. (1994): Annite stability revised: 1. Hydrogen-sensor data for the reaction annite = sanidine + magnetite + H_2. *Contrib. Mineral. Petrol.* **117**, 229–240.

Donnay, G., Donnay, J.D.H. and Takeda, H. (1964): Trioctahedral one-layer Micas. II Prediction of the structure from composition and cell dimensions. *Acta Cryst.* **17**, 1341–1381.

Dyar, M.D. (1987): A review of Mössbauer data on trioctahedral micas: Evidence for tetrahedral Fe^{3+} and cation ordering. *Am. Mineral.* **72**, 792–800.

Eugster, H.P. (1957): Stability of annite. Carnegie Institution of Washington Yearbook, 1956–57, 161–164.

Eugster, H.P. and Wones, D.R. (1962): Stability relations of the ferruginous biotites annite. *J. Petrol.* **3**, 82–126.

Farmer, V.C. (1974): The layer silicates. In: Farmer, V.C. (ed.): The infrared spectra of minerals. Mineral. Soc. Great Britain, London, 331–363.

Farmer, V.C, Russell, J.D. and McHardy, W.J. (1971): Evidence for loss of protons and octahedral iron from oxidized biotites and vermiculites. *Mineral. Mag.* **38**, 122–137.

Gilkes, R.J., Young, R.C. and Quirk, J.P. (1972): The oxidation of octahedral iron in biotite. *Clays Clay Mineral.* **20**, 303–315.

Guidotti, C.V. and Dyar, M.D. (1991): Ferric iron in metamorphic biotite and it's petrologic and crystallochemical implications. *Am. Mineral.* **76**, 161–175.

Hamilton, D.L. and Henderson, C.B.M. (1968): The preparation of silicate compositions by gelling method. *Mineral. Mag.* **36**, 632–838.

Hazen, R.M. and Burnham, C.W. (1973): The crystal structure of one-layer phlogopite and annite. *Am. Mineral.* **58**, 889–900.

Ishii, M., Shimanouchi, T. and Nakahira, M. (1967): Far infrared absorption spectra of layer silicates. *Inorg. Chim. Acta* **1**, 387–392.

Ishii, M., Nakahira, M. and Takeda. H. (1969): Far infrared absorption spectra of micas. Proc. Int. Clay Conf., **1**, 247–259.

Jenkins, D.M. (1989): Empirical study of the infrared lattice vibrations (1100–350 cm^{-1}) of phlogopite. *Phys. Chem. Mineral.* **16**, 408–414.

Laperche, V. (1991): Étude de l'état et de la localisation des cations compensateurs dans les phyllosilicates. Thèse de 3ème cycle, Univ. Paris VII, 104 pp.

Levillain, C. (1982): Influence des substitutions cationiques et anioniques majeurs sur les spectres Mössbauer et Infrarouge des micas potassiques trioctaédriques. Applications cristallochimiques. Thèse d'Etat, Univ. Paris VI, 158 pp.

Levillain, C. and Maurel, P. (1980a): Étude par spectrométrie infrarouge des fréquences d'élongation du groupement hydroxyl dans des micas synthétiques de la série annite-phlogopite et annite-sidérophyllite. *C. R. Acad. Sci. Paris* **290**, 1289–1292.

Levillain, C. and Maurel, P. (1980b): Étude par spectrométrie infrarouge de l'influence de la liaison hydrogène sur les fréquences d'élongation des liaisons Si–O dans les micas potassiques. *C. R. Acad. Sci. Paris* **290**, 1385–1388.

Liu, X.F. (1989): Significations pétrogénétique des micas trioctaédriques sodiques. Modélisation expérimentale dans le système NaO_2-K_2O-MgO-Al_2O_3-SiO_2-H_2O-(TiO_2-HF-D_2O). Thèse de 3ème cycle, Univ. Orléans, 105 pp.

McKoewn, D.A., Bell, M.I. and Etz, E.S. (1999): Raman spectra and vibrational analysis of the trioctahedral mica phlogopite. *Am. Mineral.* **84**, 970–976.

Monier, G. and Robert, J.-L. (1986): Muscovite solid solution in the system K_2O-MgO-FeO-Al_2O_3-SiO_2-H_2O: An experimental study at 2 kbar P_{H2O} and comparison with natural Li-free white micas. *Mineral. Mag.* **50**, 257–266.

Nachit, H. (1986): Contribution à l'étude analytique et expérimentale des biotites des granitoïdes - applications typologiques. Thèse de 3ème cycle, Univ. Brest, 150 pp.

Papin, A., Sergent, J. and Robert, J.-L. (1997): Intersite OH:F distribution in an Al-rich phlogopite. *Eur. J. Mineral.* **9**, 501–508.

Partin, E. (1984): Ferric/Ferrous determination in synthetic biotite. M.S Thesis, Virginia Polytechnic Institute and State University, Blacksburg.

Rebbert, C.R., Partin, E. and Hewitt, D.A. (1995): Synthetic biotite oxidation under hydrothermal conditions. *Am. Mineral.* **80**, 345–354

Redhammer, G.J., Beran, A., Dachs, E. and Amthauer, G. (1993): A Mössbauer and X-Ray diffraction study of annites synthesized at different oxygen fugacities and crystal chemical implications. *Phys. Chem. Mineral.* **20**, 382–394.

Redhammer, G.J., Beran, A., Schneider, J., Amthauer, G. and Lottermoser, W. (2000): Spectroscopic and structural properties of synthetic micas on the annite-siderophyllite binary: Synthesis, crystal structure refinement, Mössbauer, and infrared spectroscopy. *Am. Mineral.* **85**, 449–465.

Robert, J.-L. (1973): Étude expérimentale de micas dans le système K_2O-MgO-TiO_2-Al_2O_3-SiO_2-H_2O. Thèse de 3ème cycle, Univ. de Paris-Sud, 55 pp.

Robert, J.-L. (1976): Phlogopite solid solutions in the system K_2O-MgO-Al_2O_3-SiO_2-H_2O. *Chem. Geol.* **17**, 195–212.

Robert, J.-L. (1981): Études cristallochimiques sur les Micas et les Amphiboles – Applications à la Pétrographie et à la Géochimie. Thèse d'Etat, Univ. de Paris Sud Orsay, 206 pp.

Robert, J.-L. and Maury, C.R. (1979): Natural occurence of a (Fe, Mn, Mg) tetrasilicic potassium mica. *Contrib. Mineral. Petrol.* **68**, 117–123.

Robert, J.-L., Beny, J.-M., Della Ventura, G. and Hardy, M. (1993): Fluorine in micas: crystal-chemical control of the OH–F distribution between trioctahedral and dioctahedral sites. *Eur. J. Mineral.* **5**, 7–18.

Rousseaux, J.M., Gomez Laverde, Y., Nathan, Y. and Rouxet, P.G. (1972): Correlation between the hydroxyl stretching bands and the chemical compositions of the trioctahedral micas. Int. Clay Conf. Madrid, Preprint, 1, 117–126.

Russell, J.D., Farmer, V.C. and Velde, B. (1970): Replacement of OH by OD in layer silicates, and identification of the vibrations of these groups in infrared spectra. *Mineral. Mag.* **37**, 869–879.

Rutherford, M.J. (1973): The phase relations of aluminous iron biotites in the system $KAlSi_3O_8$-$KAlSiO_4$-Al_2O_3-Fe-O-H. *J. Petrol.* **14**, 159–80.

Sabatier, H. (1974): Étude de quelques micas tri- et tétrasiliciques dans le système K-Fe-Si-O-H. Comparaison avec les biotites vertes naturelles. Thèse de 3ème cycle , Univ. de Paris VI, 116 pp.

Sanz, J. (1976): Ordre-désordre dans la couche octaédrique des micas trioctaédriques. Étude par résonance magnétique nucléaire, Infrarouge et Mössbauer. Thèse, Univ. Cath. Louvain, Belgique.

Sanz, J., Meyers, J., Vielvone, L. and Stone, W.E.E. (1978): The location and content of iron in naturel biotites and phlogopite: A comparison of severals methodes. *Clay Mineral.* **13**, 45-52.

Schroeder, P.A. (1990): Far infrared, X-Ray powder diffraction and chemical investigations of potassium micas. *Am. Mineral.* **75**, 983–991.

Tateyama, H., Shimoda, S. and Sudo, T. (1977): Estimation of K–O distance and tetrahedral rotation angle of K-micas from far-infrared absorption spectral data. *Am. Mineral.* **62**, 534–539.

Vedder, W. (1964): Correlation between Infrared spectrum and chemical composition of micas. *Am. Mineral.* **49**, 736–768.

Velde, B. (1978): Infrared spectra of synthetic micas in the series muscovite-MgAl celadonite. *Am. Mineral.* **63**, 343–3

Velde, B. (1979): Cation-apical oxygen vibrations in mica tetrahedra. *Bull. Mineral.* **102**, 33–34.

Velde, B. (1983): Infrared OH-stretch bands in potassic micas, talcs and saponites; influence of electronic configuration and site of charge compensation. *Am. Mineral.* **68**, 1169–1173.

Wilkins, R.W.T. (1967): The hydroxyl-stretching region of biotite mica spectrum. *Mineral. Mag.* **36**, 325–333.

Wones, D.R. (1963a): Phase equilibria of ferriannite $KFe^{2+}{}_3Fe^{3+}Si_3O_{10}(OH)_2$. *Am. J. Sci.* **262**, 918–929.
Wones, D.R. (1963b): Physical properties of synthetic biotites on the join phlogopite-annite. *Am. Mineral.* **48**, 1300–1321.
Wones, D.R. and Eugster, H.P. (1965): Stability of biotite: experiment, theory and application. *Am. Mineral.* **50**, 1228–1272.

Received 11 July 2002
Accepted in revised form 4 November 2002
Editorial handling: Th. Armbruster